A Thiosemicarbazone-Nickel(II) Complex as Efficient Electrocatalyst for Hydrogen Evolution

Tatiana Straistari, Jennifer Fize, Sergiu Shova, Marius Réglier, Vincent Artero, Maylis Orio

A thiosemicarbazone-nickel(II) complex as efficient electrocatalyst for hydrogen evolution

Tatiana Straistari,[a,b] Jennifer Fize,[c] Sergiu Shova,[d] Marius Réglier,[a] Vincent Artero*[c] and Maylis Orio*[a]

Dedicated in memory of Prof. Constantin Turta for his outstanding contribution to inorganic and coordination chemistry

Abstract: We report herein on of the synthesis and characterization of a new mononuclear nickel complex **NiL** based on a thiosemicarbazone ligand that exhibits an electrocatalytic behavior for H_2 evolution in DMF using trifluoroacetic acid (TFA) as the proton source. A maximum turnover frequency (TOF_{max}) of 3080 s^{-1} was extrapolated for 1 M proton concentration using the *foot-of-the wave analysis* of cyclic voltammetry data. Gas analysis during controlled potential electrolysis experiments confirmed the catalytic nature of the process and production of dihydrogen with 80% faradaic yield. Quantum chemical calculations indicate that the catalytic mechanism involves first ligand-based reduction and protonation steps followed by metal-centered processes.

Introduction

Facing the 21st century energy challenge, dihydrogen production as an alternative fuel by catalytic water splitting is a central theme in the field of renewable energy storage.[1] Platinum possesses the best performances among catalysts able to reduce protons to dihydrogen.[2] However, due to its scarcity and its cost, efforts to find alternative non-noble transition metal catalysts have been the subject of intense research.[3-6] Inspiration by nature has often guided these researches. For example, some of us recently reported a heterobinuclear NiFe complex reproducing the structure of the active site of [NiFe]-hydrogenase,[7] and exhibiting high rates for electrocatalytic H_2 evolution in mildly acidic solutions.[8] Besides such biomimetic approaches, a number of molecular catalysts based on Earth-abundant metals have been developed in the recent years and were benchmarked with the so-called "catalytic Tafel plots".[9] Together with the introduction of proton relays in the second coordination sphere of the metal center,[10,11] redox-active ligands[12] can be exploited to promote or enhance catalytic activity.[13-16] Transition metal complexes with *bis*-thiosemicarbazone ligands have been studied for many years.[17] Beyond their interest as chemotherapeutics or radiopharmaceutics,[18] these complexes present some interesting features (redox properties, nitrogen or sulfur atoms as potential proton relays) that could be relevant for electrocatalytic proton reduction. Recently, Haddad *et al.* have reported a bis-thiosemicarbazone zinc complex that functions as a homogeneous electrocatalyst for proton reduction,[16] and analyzed its reactivity in terms of ligand-centered[15] [19,20] proton-transfer and electron-transfer processes shortcutting traditional metal-hydride intermediates. In that perspective, we associated the electroactive *bis*-thiosemicarbazone ligand with redox-active transition metal and report here the synthesis and characterization of a *bis*-thiosemicarbazone nickel(II) complex together with its evaluation as an electrocatalyst for proton reduction.

Results and Discussion

Synthesis of the ligand and complex

The 4–{bis(4–(p–methoxyphenyl)–thiosemicarbazone)}–2,3-butane ligand (**H_2L**) used in this study was quantitatively prepared by the reaction of 2,3-dihydrazide-butane with two equivalents of 1-isothiocyanato-4-methoxy-benzene in refluxing ethanol. **H_2L** precipitated from ethanol as a yellow-orange powder in 93% yield and was used further without any additional purification, except washing with ethanol. The addition of one equivalent of nickel nitrate to a suspension of **H_2L** in methanol, resulted in the formation of the **NiL** nickel complex in good yield (65%). The crude compound precipitated as a dark brown microcrystalline powder and did not required any purification, except washing with methanol. **H_2L** and **NiL** were fully characterized by elemental analyses, infra-red and ^{1}H NMR spectroscopies and their structures were confirmed by X-ray crystallography.

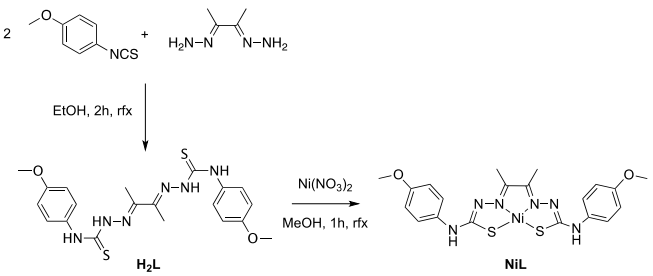

Scheme 1. Synthesis of **H_2L** and **NiL**.

[a] T. Straistari, Dr. M. Réglier, Dr. M. Orio
Aix Marseille Univ, CNRS, Centrale Marseille, iSm2, Marseille, France
E-mail: maylis.orio@univ-amu.fr
[b] T. Straistari
Institute of Chemistry, Academy of Sciences of Moldova
3, Academiei str., Chisinau MD 2028, Republic of Moldova
[c] J. Fize, Dr. V. Artero
Univ. Grenoble Alpes, CNRS UMR 5249, CEA, Laboratoire de Chimie et Biologie des Métaux, 38000 Grenoble, France
E-mail: vincent.artero@cea.fr
[d] Dr. S. Shova
Institute of Macromolecular Chemistry "Petru Poni", 41A Grigore Ghica Voda Alley, Iasi-700487, Romania

Supporting information for this article is given via a link at the end of the document.((Please delete this text if not appropriate))

X-ray Crystallography

Crystals of **H_2L**, [NiL]·2.5DMF and [NiL]·2DMSO compounds suitable for X-ray analysis were grown from DMF. **H_2L** crystallizes in triclinic *P*-1 space group and its structure consists of 4–{bis (4–(p–methoxyphenyl)–thiosemicarbazone)}–2,3-butane molecule (Figure SI-1 and SI-2) as the asymmetric part of the unit cell. The results of single crystal X-ray study for [NiL] 2.5DMF and [NiL]·2DMSO complexes are shown in Figures 1 and SI-3, respectively. Since both complexes exhibit similar molecular structures (Table SI-1), only the crystal structure of [NiL]·2.5DMF will be described. The assymmetric unit contains two crystallographically distinct but chemically identical **NiL** neutral complexes (denoted A and B) and 5 DMSO as solvated molecules. Each Ni atom has a distorted square-planar N_2S_2 coordination geometry provided by tetradentate doubly deprotonated ligand L^{2-}. Both NiN_2S_2 fragments are essentially planar within 0.003 and 0.002 Å distortion for A and B molecules, respectively. As a whole, both independent **NiL** units are also almost planar being arranged in parallel fashion with an interplanar angle of 1.33º. Selected bond lengths are provided in the caption of Figure 1.

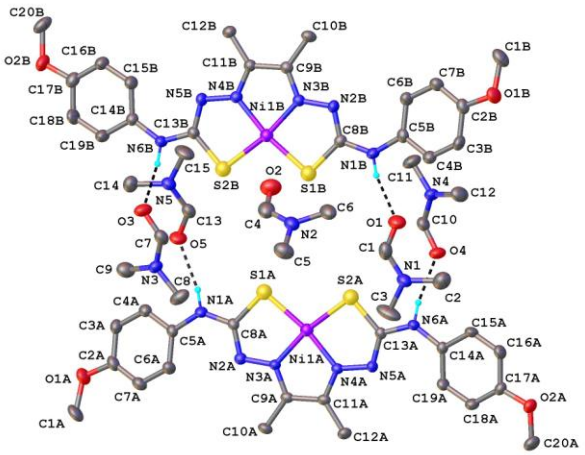

Figure 1. Asymmetric part in the crystal structure of **[NiL]·2**.5DMF with atom labeling scheme and ellipsoids parameters at 50% probability level. H-atoms not involved in hydrogen bonds are omitted for clarity Selected bond lengths: Ni(1B) − S(1B) 2.170(4) Å, Ni(1B) − S(2B) 2.167(4) Å, Ni(1B) − N(3B) 1.80(1) Å, Ni(1B) − N(4B) 1.85(1) Å, Ni(1A) − S(1A) 2.165(5) Å, Ni(1A) − S(2A) 2.170(5) Å, Ni(1A) − N(3A) 1.82(1) Å, Ni(1A) − N(4A) 1.84(2) Å. Hydrogen bonds parameters: N1A−H···O5 [N1A−H 0.86 Å, H···O5 2.09 Å, N1A···O5 2.921(3) Å, N1A−H···O5 163.2°]; N6A−H···O4 [N6A−H 0.86 Å, H···O4 2.11 Å, N6A···O4 2.932(3) Å, N6A−H···O4 163.3°]; N1B−H···O1 [N1B−H 0.86 Å, H···O1 1.97 Å, N1B···O1 2.805(3) Å, N1B−H···O1 164,9°]; N6B−H···O3 [N6B−H 0.86 Å, H···O3 2.02 Å, N6B···O3 2.848(3) Å, N6B−H···O3 160.2°]

Electrochemical Studies

Cyclic voltammograms (CV) were recorded at a glassy carbon electrode in anhydrous DMF in the presence of 0.1M NBu_4PF_6 as supporting electrolyte. Potentials are referred to a Ag/AgCl reference electrode. The redox behavior of **H_2L** was investigated first. In the potential range between +0.8 and -2.0 V vs Ag/AgCl, the CV of **H_2L** and its deprotonated form **L^{2-}**, formed *in situ* through reaction with Et_3N,revealed no oxidative processes, while an irreversible wave corresponding to the reduction of the imine functions is observed at -1.65 V vs Ag/AgCl (Figure SI-4).[21] This wave is more intense in the deprotonated ligand. To study the behavior of the ligand in acid medium, we recorded successive cyclic voltammograms of **H_2L** in DMF in the presence of trifluoroacetic acid. Scans in the negative direction from 0 to -2 V vs Ag/AgCl revealed no catalytic wave

Figure 2 shows the CV of **NiL** in anhydrous DMF under argon. It revealed two successive reversible one-electron redox systems at – 1.04 V ((E_{pc}* + E_{pa}*)/2) and –1.67 V vs Ag/AgCl ((E_{pc}** + E_{pa}**)/2).

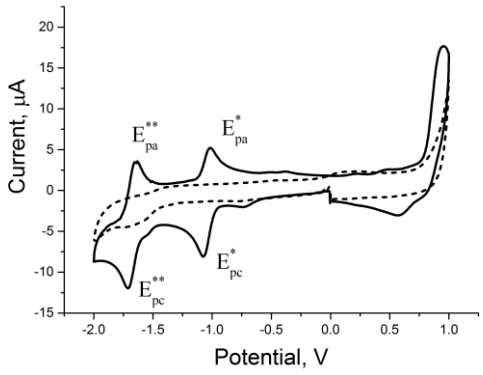

Figure 2. Cyclic voltammograms of **H_2L** (black dashed line) and **NiL** (black plain line), (1 mM) at a stationary glassy carbon electrode in DMF + 0.1M NBu_4PF_6. Scan rate 500mV/s. Potentials are referenced to the Ag/AgCl electrode

A plot of the current peaks *versus* the square root of the scan rates for both waves is linear, indicating that is a diffusion-controlled process (Figure SI-5). In an effort to understand the redox behavior of **NiL**, DFT calculations were undertaken. The structures of **NiL**, **NiL^-** and **NiL^{2-}** were subjected to geometry optimization (Figure SI-9) and their electronic structures were investigated (Figures 3 and SI-10). Comparison of the DFT-optimized structure of **NiL** with the X-ray data showed a pretty good agreement between the two sets of data which confirmed that **NiL** can be best described as a low spin Ni(II) complex ($[Ni^{II}L]^0$, S = 0). Looking at the one-electron reduced species, a delocalized ligand-based radical species ($[Ni^{II}L^{\bullet}]^-$, S = ½) is formed upon reduction of **NiL** as the singly occupied molecular orbital (SOMO) of **NiL^-** is essentially distributed over the hydrazone bridge of the complex. The second reduction process in **NiL** occurs at the metal site leading to the formation of Ni(I) as the second SOMO of **NiL^{2-}** is mainly distributed on the nickel center and its coordinating atoms. Due to the orthogonality of the two SOMOs of **NiL^{2-}** and an energy gap of 25 kcal.mol^{-1} with respect to the singlet state, the ground spin state of this species can be assigned as a triplet ($[Ni^{I}L^{\bullet}]^{2-}$, S =1) (See the supporting information). These data thus support the experimental assignment of the reduction loci in **NiL**.

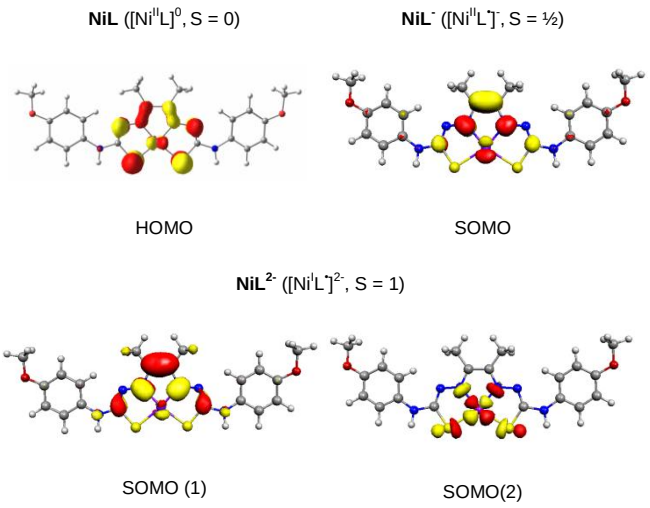

Figure 3. DFT-calculated redox active orbitals for neutral, mono and di-reduced species of **NiL**.

UV-Visible Spectroscopy and Spectroelectrochemistry

UV/Vis absorption spectra recorded in DMF for **NiL** complex exhibit an intense band at λ_{max} = 470 nm (ε = 17000, Figure 4). The electrochemical reduction of **NiL**, at room temperature was monitored spectro-electrochemically using an optically transparent electrode under Ar in DMF containing NBu_4PF_6 (0.1 M) as supporting electrolyte. After applying the potential of the first reduction band (E_{pc}*), we observed a slight decrease in intensity of the band associated with the **NiL** complex (green line), and after further electrochemical re-oxidation (E_{pa}*), the band returned to the original shape (red line). Strong decrease in intensity of the band is observed after second electrochemical reduction (E_{pc}**, blue line). After total electrochemical re-oxidation (E_{pa}*), the intensity of the band returned to the initial one. This behavior strongly confirms the reversibility of the redox electrochemical processes.

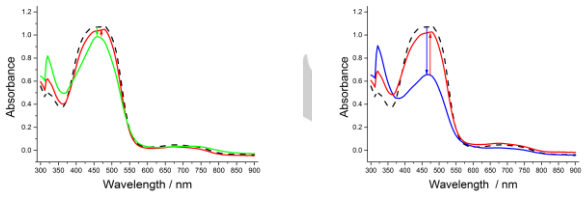

Figure 4. Electronic absorption spectra for **NiL** (black dash), one-electron reduced specie **NiL**$^-$ (green line), two-electron reduced species **NiL**$^{2-}$ (blue line), and electrochemical re-oxidized species (red lines).

TDDFT calculations performed on neutral, mono and di-reduced forms of **NiL** further supported that the UV-vis spectrum of the complex is dominated by one main absorption band in all three redox states. This band could be assigned to (i) a mixed metal-ligand to metal-ligand transition for **NiL**; (ii) a metal to ligand transition in **NiL**$^-$ and (iii) to a ligand-to-ligand charge transfer in **NiL**$^{2-}$ (Table SI-3 and Figure SI-12). Our calculations also show a decrease in the intensity of the band for the direduced compound, consistently with the experimental observation (Figure SI-11).

Electrocatalysis

To examine the capability of **NiL** to mediate proton reduction catalysis, we investigated its electrochemical response in the presence of trifluoroacetic acid (TFA, pK_a = 6.0 ± 0.3 in DMF)[22] as a protons source. Cyclic voltammograms of **NiL** recorded in DMF with increasing concentration of TFA are shown in Figure SI-6. A large irreversible catalytic wave starting at about – 0.70 V *vs.* Ag/AgCl is observed. The current response of this irreversible cathodic wave is directly proportional to the concentration of protons in the electrolyte solution while the peak maximum is gradually shifted of from – 1.57 to – 1.77 V vs Ag/AgCl. Comparison with a control experiment measured in the absence of NiL demonstrate the catalytic effect of the nickel complex.. The wave displays several shoulders indicative several mechanisms operating at different potentials. We only investigate here the process occurring at more positive potentials with a mid-wave potential (E^0_{cat}) of -0.8 V vs Ag/AgCl, (Figure 5).

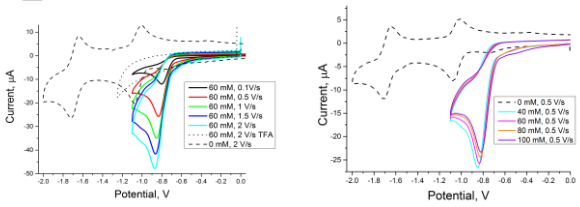

Figure 5. Successive cyclic voltammograms recorded at a glassy carbon electrode of a 1mM solution of **NiL** complex in DMF (0.1 M NBu_4PF_6) with 60 mM TFA at 5 different scan rates (left) and increasing concentration of TFA at 500mV/s scan rate (right). Potentials are referenced to the Ag/AgCl electrode.

Bulk electrolysis and gas analysis

To confirm that the catalytic wave corresponds to the reduction of protons to molecular hydrogen, we performed a bulk electrolysis experiment on a mercury pool electrode in DMF in the presence of TFA. This experiment was coupled with in-line GC analysis. During a 16 h electrolysis experiment of a 1 mM **NiL** DMF solution (0.1 M NBu_4PF_6, 8 mL) added with 100 mM TFA at – 1.2 V *vs.* Ag/AgCl, hydrogen was produced with 80 % faradaic efficiency and a turnover number of 21 (Figure SI-8). A control experiment performed in the absence of **NiL** produced significantly less hydrogen (Figure SI-6). These experiments allow to rule out the possibility that proton reduction occurs as the result of deposition of nickel nanoparticles on the electrode surface since they would amalgamate within the mercury pool electrode.

Kinetic analysis and benchmarking of performances

The *foot-of-the-wave analysis* (FOWA) was used to quantify the rates of the hydrogen evolution reaction from CV measurements.[9,23]

Plotting i/i_P^0 (with i_P^0 being the peak current of a monoelectronic wave measured in the absence of acid) as a function of $1/(1+\exp F/RTE-Ecat0$ near the foot of the wave gave a linear function at a given scan rate. The observed rate constant k_{cat} can be extracted from the slope of the linear fit, considering the formula corresponding to an ECEC mechanism (E corresponds to an electron transfer step and C to a chemical reaction, here protonation) as shown in Scheme 2 (see below). The rate constant k_{cat} for H_2 evolution catalyzed by **NiL** was determined for 4 TFA concentrations (10, 30, 60 and 80 mM) at 4 different scan rates in the 0.5 - 2 V/s range. Our data indicated that k_{cat} was proportional to the acid concentration ($k_{cat} = k_{obs} \times [H^+]$ with k_{obs} the rate constant for the rate-determining step of the process and $[H^+]$ the concentration of the acid in the bulk solution (Table SI-2). An average value of k_{obs} = 3080 $M^{-1}s^{-1}$ (Figure SI-7) was obtained. From that value a turnover frequency of 3080 s^{-1} can be extrapolated for 1M acid concentration. Based on this value, the E_{cat}^0 value of -0.8V vs Ag/AgCl (corresponding to -1.33 V vs Fc^+/Fc) and an apparent equilibrium potential of the H^+/H_2 couple (-1.01 V vs Fc^+/Fc[24]) at 1M TFA concentration, we could derive the bold magenta trace in the catalytic Tafel plot shown in Figure 6, relating the turnover frequency and driving force of the reaction, that is, the overpotential related to H_2 evolution under the conditions used.[9, 25] Although not rivalling nickel-bisdiphosphine or cobaloxime catalysts, **NiL** complex displays significant catalytic activity (log(TOF)/s−1) > 1) for overpotential values slightly lower than iron tetraphenylporphyrin[9].

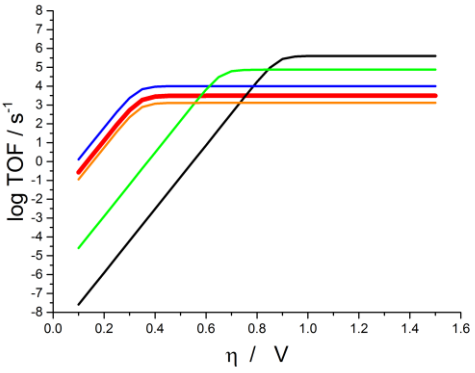

Figure 6. Catalytic Tafel plots. Comparison of performances for hydrogen evolution catalyzed by **NiL** in DMF in presence of 1 M TFA (magenta line) with those of other catalysts reported in the literature. Black: $Fe^{II}TPP$, DMF, Et_3NH^+. Blue: $Co^{II}(dmgH)_2py$, DMF, Et_3NH^+. Green: $[Ni(P_2^{Ph}N^{Ph})_2]^{2+}$, MeCN, $DMFH^+$. Orange: $[Ni^{II}(P_2^{Ph}N_2^{C6H4X})_2]^{2+}$, X= $CH_2P(O)(OEt)_2$, MeCN, $DMFH^+$. Red : $[Ni^{II}(P_2^{Ph}N_2^{C6H4X})_2]^{2+}$, X= H, MeCN, TfOH..[9]

Mechanistic considerations

To gain more insight on the locus of proton addition following the electrochemical reduction process, we have conducted additional DFT calculations. For this purpose, we have considered five potential sites for the addition of one proton on the one-electron reduced species **NiL**$^-$: the metal center [Ni-H]$^-$, the sulfur atom (generating [Ni-SH]$^-$), the nitrogen atom from the hydrazone group (generating [Ni-HN]$^-$), the internal nitrogen atom from the thiosemicarbazone motif (generating [Ni-NH]$^-$) and the nitrogen atom from the phenylthiocarbamide fragment (generating [Ni-HNH]) (Figures SI-13 and SI-15 to SI-18). Our results clearly pinpoint that the hydrazine-nitrogen is the preferential locus and can be best described as a ligand-based radical species (Figure SI-14). Indeed, the calculated free energies for the five forms predict the [Ni-HN]$^-$ form to be lower in energy by 4.0, 12.3, 18 and 21.3 kcal/mol^{-1} than the [Ni-NH]$^-$, [Ni-HNH]$^-$, [Ni-SH]$^-$ and [Ni-H]$^-$ ones, respectively (Figure 7). The preferential locus for the successive reduction of the one-electron protonated species was also investigated (Figures SI-20 and SI-22 to SI-25) and the theoretical data show that the favored species is the di-reduced [Ni-HN]$^{2-}$ complex (Figure SI-19). Our calculations also indicate that this reduction is a metal-based process as positive spin population is found at the Ni center (Figure SI-21). This would support the metal as being the preferential locus for the second protonation of [Ni-HN]$^{2-}$, generating a Ni^{III}-hydride species as the catalytically active species responsible for H_2 evolution.

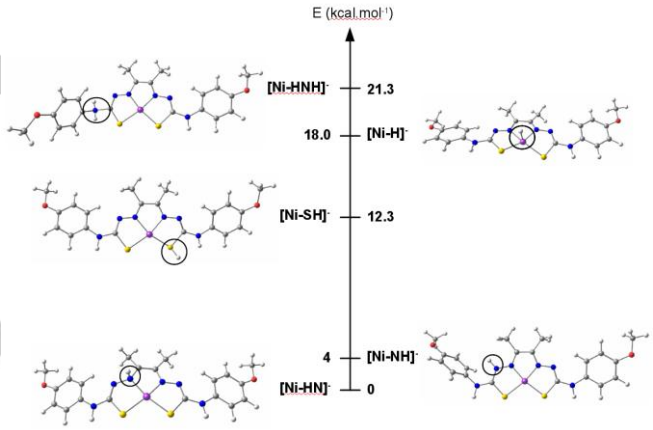

Figure 7. Energetic stability of protonated species of **NiL**$^-$

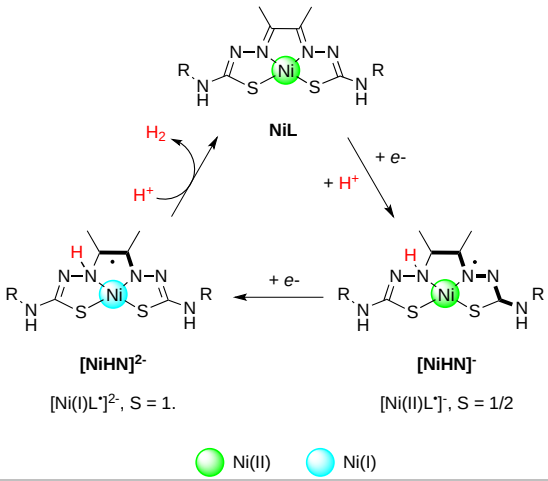

Scheme 2. Proposed mechanism for H_2 evolution.

Conclusions

In summary, we have shown that the mononuclear nickel complex **NiL** with bis-thiosemicabazone ligand exhibits a high electrocatalytic activity for proton reduction to dihydrogen. The benchmarking of the performances of **NiL** was achieved through *foot-of-the-wave analysis*[9] leading to a maximum turnover frequency 3080 s^{-1} (TOF_{max}) placing NiL among the best catalyst reported in the literature in catalytic Tafel plots. With the help of DFT calculations, we could proposed a mechanism involving two steps: 1) the protonation of the N-atom from the hydrazone function of a mono-reduced species and 2) a second reduction associated with a nickel centred protonation for subsequent hydrogen evolution.

Recently; Grapperhaus and coworkers reported a bis-thiosemicabazone zinc complex capable of electrocatalytic proton reduction through a process entirely centered on the ligand,[16] i.e. without any occurrence of a zinc hydride species. This was confirmed by the activity of the ligand alone, which exhibits a quite high TOF (1320 s^{-1}) compared to the zinc complex (1170 s^{-1}). Grapperhaus and colleagues argued that in transition-metal complexes, spin-orbit coupling between ligand-based radical and unpaired electrons from the metal can reduce reactivity. Our ligand L^{2-} appears to be deprived of any catalytic activity for H_2 evolution. With a TOF_{max} of 3080 s^{-1} for **NiL**, our results however confirm the interest to combine electroactive ligand such as bis-thiosemicarbazone with a transition metal ion to obtain a synergistic effect with both redox moieties.

Experimental Section

All solvents and chemicals were purchased from Sigma Aldrich and used without further purification. Syntheses of 1-isothiocyanato-4-methoxy-benzene and 2,3-dihydrazide-butane were performed according to procedures described by Demchenko[26] and Lakshmi.[27] The synthesis of the ligand **H_2L** is presented in ESI. ^{1}H NMR spectra were recorded on Bruker 400MHz Avance III nanobay. Chemical shifts for ^{1}H NMR spectra are referenced relative to TMS or the residual protonated solvent. IR spectra were recorded with Bruker TENSOR 27 spectrometer equipped with a single-reflection DuraSamplIR diamond. Elemental analysis was performed on Thermo Finnigan EA 1112 instrument. The results were validated by at least two sets of measurements.

Synthesis of H_2L

Synthesis of 4–{bis(4–(p–methoxyphenyl)–thiosemicarbazone)}–butane ligand (H_2L). The 2,3-dihydrazide-butane (4.382 mmol; 0.5 g) was dissolved in ethanol (20 ml), and then added dropwise to two equivalents of 1-isothiocyanato-4-methoxy-benzene solution in ethanol (10 ml). The mixture was heated at reflux for 2 h. After the reaction mixture was cooled to room temperature, the yellow solid was filtered and washed with two portions of ethanol to give 93% yield of crude compound that was used for the complexation step whitout additional purification. Selected data for ligand: ^{1}H NMR (400 MHz, [D_6]DMSO, TMS): δ = 10.55 (s, 2H; NH), 9.89 (s, 2H; NH), 7.38 (d, *J* = 9 Hz, 4H; *o*-CH), 6.93 (d, *J* = 9 Hz, 4H; *p*-CH), 3.76 (s, 6H; O-CH_3), 2.30 ppm (s, 6H; CH_3). FT-IR: 3209 cm^{-1} (N−H), 1593 cm^{-1} (C=N imine), 1510 (N−C) cm^{-1}, 1240 cm^{-1} and 1026 cm^{-1} (O−C), 829 cm^{-1} (C=S). Elemental analysis: calcd. (%) for $C_{20}H_{24}N_6O_2S_2$ (444.57): C 54.03, H 5.44, N 18.90, S 14.43; found: C 54.10, H 5.37, N 18.89, S 14.36

Synthesis of NiL

To the suspension of ligand **H_2L** (0.225 mmol, 0.1 g) in methanol (5 ml), wad added drop-wise one equivalent of $Ni(NO_3)_2(H_2O)_6$ (0.225 mmol, 0.065 g) solution in methanol (2 ml). The resulting suspension was stirred at reflux for 2 hours. The resulting precipitate was filtrated and washed with methanol. Single crystals suitable for crystallographic analysis were grown from DMF solution with 65 % yield. Selected data: ^{1}H NMR (400 MHz, [D_6] DMSO-d_6, TMS): δ = 9.93 (s, 2H; NH), 7.51 (d, *J* = 8.7 Hz, 4H; *o*-CH), 6.87 (d, *J* = 8.7 Hz, 4H; *p*-CH), 3.71 (s, 6H; O-CH_3), 2.04 ppm (s, 6H; CH_3);); FT-IR 3300 cm^{-1} (N−H), 1600 cm^{-1} (C=N imine), 1504 cm^{-1} (N−C), 1240 cm^{-1} and 1015 cm^{-1} (O−C), 817 cm^{-1} (C−S); elemental analysis. Calcd. $C_{20}H_{24}N_6O_2S_2Ni$ (501.25): C 47.92, H 4.42, N 16.77, S 12.79; found C 47.49, H 4.46, N 16.43, S 11.42.

X-ray crystallography

Crystallographic data for **H_2L (**CCDC-1497213), [NiL]·2.5DMF (CCDC-1497214) and [NiL]·2DMSO (CCDC-1497215) can be obtained free of charge from The Cambridge Crystallographic Data Centre via: www.ccdc.cam.ac.uk/data_request/cif. The molecule of ligand has *anti*-spatial orientations towards the substituents in the butane unity. The thiosemicarbazone substituents are oriented head to head in approximately of 180º. The dihedral angles between C14/C19 and C2/C6 aromatic rings and almost planar bis–thiosemicarbazone–2,3-butane fragment are of 17.01(7)º and 64.68(6)º, respectively. In the crystal the adjacent neutral molecules H_2L are interacting through N-H···S hydrogen bonds to form supramolecular chains in parallel orientation along *b* crystallographic axis (Figure SI-2).

Electrochemistry

Cyclic voltammetry experiments were performed using a BioLogic SP300 potentiostat and a three-electrode set-up consisting of a glassy carbon working electrode, a platinum wire counter electrode and an Ag/AgCl (KCl 3M) reference electrode. Ferrocene was used as an internal standard with $E^0(Fc^+/Fc)$ = 0.53 V vs Ag/AgCl. All studies were performed in deoxygenated DMF containing NBu_4PF_6 (0.1 M) as supporting electrolyte. Controlled potential electrolysis experiments were carried out in two-compartment cell. The volume of solution (DMF, 0.1 M NBu_4PF_6) used in the working compartment of the cell was 8 ml. The working electrode used was a pool of mercury, separated from the coiled platinum wire counter electrode by a porous frit. Bulk electrolysis solutions were purged witch N_2 gas for at least 20 min prior to electrolysis and stirred throughout bulk electrolysis experiment. During the experiment, the cell was continuously purged with nitrogen (5 mL.min^{-1}) and the output gas was analyzed at two-minute intervals in a Perkin Elmer Clarus 500 gas chromatographer using a previously described setup[28].

DFT calculations

All theoretical calculations were performed with the ORCA program package.[29] Full geometry optimizations were undertaken for all complexes using the GGA functional BP86[30] in combination with the TZV/P[31] basis set for all atoms, and by taking advantage of the resolution of the identity (RI) approximation in the Split-RI-J variant[32] with the appropriate Coulomb fitting sets[33] Increased integration grids (Grid4 in ORCA convention) and tight SCF convergence criteria were

used. Electronic structures and Molecular Orbital diagrams were obtained from single-point calculations using the hybrid functional B3LYP[34] together with the TZV/P[31] basis set. Increased integration grids (Grid4 and GridX4 in ORCA convention) and tight SCF convergence criteria were used in the calculations. For according to the experimental conditions solvent effects were accounted and we used the DMF solvent (ε = 37) within the framework of the conductor-like screening (COSMO) dielectric continuum approach.[35] The relative energies were computed from the gas-phase optimized structures as a sum of electronic energy, solvation and thermal corrections to the free energy. Optical properties were predicted from additional single-point calculations using the hybrid functional B3LYP[34] together with the TZV/P[31] basis set. Electronic transition energies and dipole moments for all models were calculated using time-dependent DFT (TD-DFT)[36] within the Tamm–Dancoff approximation.[37] To increase computational efficiency, the RI approximation[38] was used in calculating the Coulomb term, and at least 30 excited states were calculated in each case. For each transition, difference density plots were generated using the orca plot utility program and were visualized with the Chemcraft program.[39]

Acknowledgements

The authors gratefully acknowledge the support of this work by the CNRS and the Academy of Sciences of Moldova (Bilateral agreement EDC25722 2013-2014), the French National Research Agency (Labex program, ARCANE, ANR-11-LABX-0003-01); the COST Actions CM1305 ECOSTBio (Explicit Control Over Spin-States in Technology and Biochemistry) and CM1202 Perspect-H_2O (Supramolecular photocatalytic water splitting).

Keywords: nickel • redox-active ligand • bioinspiration • electrocatalyst • hydrogen evolution

[1] A. Borgschulte, *Front. Energy Res.* **2016**, *4*, 282-288.
[2] O. T. Holton and J. W. Stevenson, *Platinum Metals Review*, **2013**, *57*, 259-271.
[3] J. R. McKone, S. C. Marinescu, B. S. Brunschwig, J. R. Winkler and H. B. Gray, *Chem. Sci.*, 2014, **5**, 865-878.
[4] V. S. Thoi, Y. J. Sun, J. R. Long and C. J. Chang, *Chem. Soc. Rev.*, 2013, **42**, 2388-2400.
[5] T. R. Simmons, G. Berggren, M. Bacchi, M. Fontecave and V. Artero, Coord. Chem. Rev., 2014, 270–271, 127-150.
[6] N. Coutard, N. Kaeffer, V. Artero, Chem. Commun. 2016, DOI: 10.1039/c6cc06311j.
[7] W. Lubitz, H. Ogata, O. Rüdiger and E. Reijerse, Chem. Rev., 2014, 114, 4081-4148.
[8] D. Brazzolotto, M. Gennari, N. Queyriaux, T. R. Simmons, J. Pecaut, S. Demeshko, F. Meyer, M. Orio, V. Artero and C. Duboc, *Nat. Chem.* **2016**, DOI:10.1038/nchem.2575.
[9] V. Artero, J.-M. Saveant, *Energy Environ. Sci.* **2014**, *7*, 3808-3814.
[10] D. L. DuBois, Inorg. Chem., 2014, 53, 3935-3960.
[11] N. Kaeffer, M. Chavarot-Kerlidou and V. Artero, Acc. Chem. Res., 2015, 48, 1286–1295.
[12] Eisenberg, R.; Gray, H. B. *Inorg. Chem.* **2011**, *50*, 9741-9751.
[13] Jurss, J. W.; Khnayzer, R. S.; Panetier, J. A.; El Roz, K. A.; Nichols, E. M.; Head-Gordon, M.; Long, J. R.; Castellano, F. N.; Chang, C. J. *Chem. Sci.* **2015**, *6*, 4954-4972.
[14] Thompson, E. J.; Berben, L. A. *Angew. Chem. Int. Ed.* **2015**, *54*, 11642-11646.
[15] Haddad, A. Z.; Kumar, D.; Ouch Sampson, K.; Matzner, A. M.; Mashuta, M. S.; Grapperhaus, C. A. *J. Am. Chem. Soc.* **2015**, *137*, 9238-9241.
[16] A. Z. Haddad, B. D. Garabato, P. M. Kozlowski, R. M. Buchanan, C. A. Grapperhaus, *J. Am. Chem. Soc*. **2016**, *138*, 7844-7847.
[17] M. J. M. Campbell, *Coord. Chem. Rev*. **1975**, *15*, 279-317.
[18] B. M. Paterson and P. S. Donnelly, *Chem. Soc. Rev.* **2011**, *40*, 3005-3018.
[19] E. J. T. L. A. Berben, *Angew. Chem. Int. Ed*. **2015**, *54*, 11642-11646.
[20] J. W. Jurss, R. S. Khnayzer, J. A. Panetier, K. A. El Roz, E. M. Nichols, M. Head-Gordon, J. R. Long, F. N. Castellano, C. J. Chang, *Chem. Sci*. **2015**, *6*, 4954-4972.
[21] E. Anxolabehere-Mallart, C. Costentin, M. Fournier, S. Nowak, M. Robert, J.-M. Savean, *J. Am. Chem. Soc.* **2012,** *134*, 6104-6107.
[22] V. Fourmond, S. Canaguier, B. Golly, M. J. Field, M. Fontecave, V. Artero, *Energy Environ. Sci.* **2011**, *4*, 2417-2427
[23] N. Elgrishi, M. B. Chambers, M. Fontecave, *Chem. Sci.* **2015**, *6*, 2522-2531.
[24] V. Fourmond, P.A. Jacques, M. Fontecave and V. Artero *Inorganic Chemistry*, 2010, **49**, 10338–10347
[25] C. Costentin, S. Drouet, M. Robert and J.-M. Savéant, *J. Am. Chem. Soc.*, 2012, **134**, 11235-11242.
[26] A. M. Demchenko, V. A. Yanchenko, V. V. Kisly, M. S. Lozinskii, *Chemistry of Heterocyclic Compounds*. **2005,** *41*, 668-672
[27] B. Lakshmi, P. G. Avaji, K. N. Shivananda, P. Nagella, S. H. Manohar, K. N. Mahendra, *Polyhedron.* **2011**, *30*, 1507-1515.
[28] S. Cobo, J. Heidkamp, P.-A. Jacques, J. Fize, V. Fourmond, L. Guetaz, B. Jousselme, V. Ivanova, H. Dau, S. Palacin, M. Fontecave and V. Artero, *Nat. Mater.*, 2012, **11**, 802-807.
[29] F. Neese, Wiley Interdiscip. Rev. Comput. Mol. Sci. **2012**, *2*, 73-78.
[30] a) J. P. Perdew, *Phys. Rev. B* 1**986**, *33*, 8822–8824; b) J. P. Perdew, *Phys. Rev. B* **1986**, *34*, 7406-7406 ; c) A. D. Becke, *Phys. Rev. A* **1988**, *38*, 3098-3100
[31] A. Schäfer, C. Huber, R. Ahlrichs, *J. Chem. Phys.* **1994**, *100*, 5829-5835.
[32] F. Neese, *J. Comput. Chem.* **2003**, *24*, 1740-1747.
[33] F. Weigend, *Phys. Chem. Chem. Phys.* **2006**, *8*, 1057-1065.
[34] a) A. D. Becke, *J. Chem. Phys.* **1993**, *98*, 1372-1377; b) C. T. Lee, W.T. Yang, R. G. Parr, *Phys. Rev. B* **1988**, *37*, 785-789.
[35] A. Klamt, G. Schürmann, *J. Chem. Soc. Perkin Trans. 2* **1993**, 799-805.
[36] a) M. E. Casida in Recent Advances in Density Functional Theory, Part I (Ed.: D. P. Chong), World Scientific, Singapore, **1995**; b) R. E. Stratmann, G.E. Scuseria, M.J. Frisch, *J. Chem. Phys.* **1998**, *109*, 8218-8224; c) R. Bauernschmitt, R. Ahlrichs, *Chem. Phys. Lett.* **1996**, *256*, 454-464.
[37] a) S. Hirata, M. Head-Gordon, *Chem. Phys. Lett.* **1999**, *314*, 291-299; b) S. Hirata, M. Head-Gordon, *Chem. Phys. Lett.* **1999**, *302*, 375-382.
[38] F. Neese, J. Chem. Phys. 2001, 115, 11080-11080.
[39] Chemcraft, http://chemcraftprog.com.

FULL PAPER

A mononuclear nickel complex **NiL** based on a thiosemicarbazone ligand is an efficient electrocatalyst for H_2 evolution in DMF. With a maximum turnover frequency of 3080 s^{-1}, it ranks among the best molecular H_2-evolving catalysts in catalytic Tafel plot. The catalytic mechanism involves ligand-based reduction and protonation steps followed by metal-centered processes.

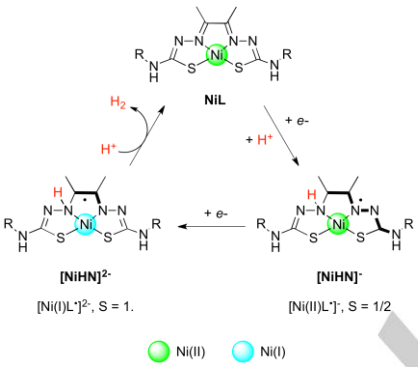

T. Straistari, J. Fize, S. Shova, M. Réglier, V. Artero, M. Orio**

Page No. – Page No.

Title